CaV1.3 L-type Ca2+ channel contributes to the heartbeat by generating a dihydropyridine-sensitive persistent Na+ current

Futoshi Toyoda, Pietro Mesirca, Stefan Dübel, Wei-Guang Ding, Joerg Striessnig, Matteo E. Mangoni, Hiroshi Matsuura

SCIENTIFIC REPORTS

OPEN

$Ca_V1.3$ L-type Ca^{2+} channel contributes to the heartbeat by generating a dihydropyridine-sensitive persistent Na^+ current

Received: 17 March 2017
Accepted: 7 July 2017
Published online: 11 August 2017

Futoshi Toyoda[1], Pietro Mesirca[2,3,4], Stefan Dubel[2,3,4], Wei-Guang Ding[1], Joerg Striessnig[5], Matteo E. Mangoni[2,3,4] & Hiroshi Matsuura[1]

The spontaneous activity of sinoatrial node (SAN) pacemaker cells is generated by a functional interplay between the activity of ionic currents of the plasma membrane and intracellular Ca^{2+} dynamics. The molecular correlate of a dihydropyridine (DHP)-sensitive sustained inward Na^+ current (I_{st}), a key player in SAN automaticity, is still unknown. Here we show that I_{st} and the L-type Ca^{2+} current ($I_{Ca,L}$) share $Ca_V1.3$ as a common molecular determinant. Patch-clamp recordings of mouse SAN cells showed that I_{st} is activated in the diastolic depolarization range, and displays Na^+ permeability and minimal inactivation and sensitivity to $I_{Ca,L}$ activators and blockers. Both $Ca_V1.3$-mediated $I_{Ca,L}$ and I_{st} were abolished in $Ca_V1.3$-deficient ($Ca_V1.3^{-/-}$) SAN cells but the $Ca_V1.2$-mediated $I_{Ca,L}$ current component was preserved. In SAN cells isolated from mice expressing DHP-insensitive $Ca_V1.2$ channels ($Ca_V1.2^{DHP-/-}$), I_{st} and $Ca_V1.3$-mediated $I_{Ca,L}$ displayed overlapping sensitivity and concentration–response relationships to the DHP blocker nifedipine. Consistent with the hypothesis that $Ca_V1.3$ rather than $Ca_V1.2$ underlies I_{st}, a considerable fraction of $I_{Ca,L}$ was resistant to nifedipine inhibition in $Ca_V1.2^{DHP-/-}$ SAN cells. These findings identify $Ca_V1.3$ channels as essential molecular components of the voltage-dependent, DHP-sensitive I_{st} Na^+ current in the SAN.

Heart automaticity is generated by the spontaneous excitation of sinoatrial node (SAN) pacemaker cells. Spontaneous activity is due to the presence of the diastolic depolarization, which leads the membrane voltage from the end of the repolarization phase to the threshold of the following action potential. There has long been considerable debate regarding the ionic mechanisms underlying diastolic depolarization, reflecting the complex nature of this physiological process. Diastolic depolarization requires a net inward current, which results from the relative balance between the decaying outward delayed rectifier K^+ currents (I_{Kr} and I_{Ks}) and the growing inward currents (see Mangoni and Nargeot for review[1]). Previous studies have identified several voltage-gated inward currents activated in the diastolic depolarization range, including the hyperpolarization-activated inward current (I_f)[2], the L- and T-type Ca^{2+} currents ($I_{Ca,L}$ and $I_{Ca,T}$)[3,4] and the sustained inward Na^+ current (I_{st})[5]. Additionally, recent experimental evidence has supported an alternative mechanism to promote pacemaker activity, in which spontaneous local Ca^{2+} release from intracellular Ca^{2+} stores stimulates electrogenic Na^+–Ca^{2+} exchanger (I_{NCX}) activity to depolarize the membrane voltage during diastolic depolarization[6]. Thus, multiple inward current systems rather than a single pacemaker current are responsible for the spontaneous activity in the SAN.

Selective pharmacological block or genetic ablation of ion channels has been extensively used to describe the contribution of ionic currents to pacemaker activity. The molecular correlates of most cardiac ionic currents have been identified allowing the development of genetically modified mouse models targeting specific ion channels including HCN4-[7,8], HCN2-I_f[9,10], $Ca_V1.3$-$I_{Ca,L}$[11,12], $Ca_V3.1$-$I_{Ca,T}$[13] and Ncx1-I_{NCX}[14]. By contrast, the complete lack

[1]Department of Physiology, Shiga University of Medical Science, Otsu Seta-Tsukinowa, Shiga, 520-2192, Japan. [2]CNRS, UMR-5203, Institut de Génomique Fonctionnelle, Département de Physiologie, LabEx ICST, Montpellier, F-34094, France. [3]INSERM, 1191, Montpellier, F-34094, France. [4]Université de Montpellier, UMR-5203, Montpellier, F-34094, France. [5]Department of Pharmacology and Toxicology, Institute of Pharmacy, Center for Molecular Biosciences, University of Innsbruck, Innsbruck, Austria. Correspondence and requests for materials should be addressed to F.T. (email: toyoda@belle.shiga-med.ac.jp)

of knowledge about the molecular determinants of I_{st} has so far prevented the evaluation of the physiological role of this important ionic current.

I_{st} was reported as a novel inward current in SAN cells of several mammalian species including rabbits, guinea-pigs, rats and mice[5,15–18]. I_{st} is activated at low membrane voltages and supplies persistent inward current flowing over the full diastolic depolarization range. Therefore, it has been proposed that this current is a physiologically important contributor to diastolic depolarization[19]. However, two decades after the first description of I_{st} by Guo *et al.*[5], there remains little progress in the identification of the molecular determinant of I_{st}. Furthermore, no specific blocker for I_{st} is available, limiting the understanding of its physiological role in SAN pacemaker activity. Although I_{st} is carried by Na^+, its pharmacological features closely resemble those of $I_{Ca,L}$: I_{st} is not affected by the voltage-gated Na^+ current (I_{Na}) blocker tetrodotoxin (TTX), but is inhibited by various chemical classes of organic Ca^{2+} channel blockers, e.g. dihydropyridines (DHPs)[5], and enhanced by the $I_{Ca,L}$ channel activator Bay-K8644[15]. Moreover, like $I_{Ca,L}$, I_{st} is also stimulated by β-adrenergic activation[5,18]. These pharmacological properties are highly specific for $I_{Ca,L}$ and suggest the possibility that the pore-forming α_1-subunit of L-type Ca^{2+} channels which carry the drug-binding domains for organic Ca^{2+}-channel blockers and activators[20,21] are also essential for I_{st} activity. Cardiac L-type Ca^{2+} channels are heteromultimers in which the pore-forming α_1 subunit associates with auxiliary subunits (in particular β, α_2/δ subunits)[22]. In SAN cells, two different α_1-subunits, $Ca_V1.2$ (α_{1C}) and $Ca_V1.3$ (α_{1D}), are expressed. $Ca_V1.2$ is uniformly expressed in heart tissue, whereas $Ca_V1.3$ is nearly absent in ventricles but is abundant in the conduction system including the SAN[12,23,24]. While $Ca_V1.3$ channels activate in the diastolic depolarization range, $Ca_V1.2$ channels are activated in the upstroke phase of the action potential[12]. In addition to forming distinct types of $I_{Ca,L}$ with different voltage dependencies of activation and inactivation, $Ca_V1.3$ and $Ca_V1.2$ channels are also differentially localized in SAN cell membranes[25].

Here we tested the hypothesis that $Ca_V1.2$ and/or $Ca_V1.3$ L-type channels are required for generating I_{st}. Using two genetically modified mouse strains we demonstrate that the $Ca_V1.3$ L-type Ca^{2+}-channel isoform is essential for functional expression of I_{st} in mouse SAN cells. Although the exact molecular mechanism linking $Ca_V1.3$ activity to I_{st} remains to be elucidated, our data show that $Ca_V1.3$ channels participate in the formation of a DHP-sensitive, voltage-dependent Na^+ conductance in SAN cells.

Results

Identification of I_{st} in mouse SAN cells. The magnitude of I_{st} varies depending on SAN cell types with distinct morphologies[5]. Mouse SAN cells used for I_{st} recordings were typically spindle- or spider-shaped with no obvious striations. These cells were small (C_m, 34.8 ± 1.2 pF, n = 42) compared to rod-shaped atrial-like cells and were spontaneously beating when superfused with normal Tyrode solution. To confirm the presence of I_{st} in these cells, the late currents elicited by 1-s depolarizing voltage-clamp steps to various test potentials from a holding potential of −90 mV were examined for the characteristics of I_{st} (Fig. 1). In order to avoid contamination of recordings by K^+ currents, we employed a Cs^+-rich internal solution. I_f was removed by substituting K^+ with Cs^+ in the external Tyrode solution, which contained 1.8 mM Ca^{2+}. To confirm the sensitivity of the sustained current to DHPs, the typical hallmark of I_{st}[19], we tested the sensitivity of the current to the potent DHP L-type Ca^{2+}-channel blocker isradipine, which has not previously been tested. In Fig. 1Aa, membrane currents recorded under control conditions (*black trace*), after lowering $[Ca^{2+}]_o$ from 1.8 to 0.1 mM (*blue trace*) and during subsequent application of 1 µM isradipine (*red trace*) are superimposed at individual test potentials. In the control bathing solution, membrane depolarization positive to −60 mV evoked a large transient inward current attributable to the activation of I_{Na} and $I_{Ca,T}$ (note that peaks are not to scale in the figure), followed by a late inward current sustained during the entire period of 1-s depolarizing pulses. An inward current with a slow current decay was observed at test potentials of > −40 mV, as expected for $I_{Ca,L}$ activation. The current-to-voltage (*I–V*) relationship obtained by plotting the current amplitude measured near the end of test pulses indicated that the late current level becomes more inward with increasing depolarization between −70 and −50 mV (*black circles*, Fig. 1Ab), generating a negative slope conductance in the range of the diastolic depolarization. Lowering external Ca^{2+} reduced a considerable fraction of $I_{Ca,L}$ at membrane voltages positive to −30 mV (*inset*, Fig. 1Aa), whereas the sustained inward current was not reduced. It is thus unlikely that the sustained inward current was generated by a window component of $I_{Ca,L}$. However, bath application of isradipine readily inhibited the sustained inward current and unmasked an almost linear background conductance (Fig. 1Aa,b). Under conditions of low $[Ca^{2+}]_o$, the DHP-sensitive sustained inward current peaked at −50 mV and the current direction was reversed at ~+26 mV (Fig. 1Ac).

Since I_{st} has been shown to be carried by Na^+[5], we tested the permeability of the sustained inward current component for Na^+. The external Na^+ was replaced with an equimolar amount of N-methyl-D-glucamine (NMDG) in the presence of 1.8 mM Ca^{2+} (Fig. 1B). Perfusion of SAN cells with Na^+-free NMDG solution readily suppressed the sustained inward current as well as Na^+-dependent background conductance (Fig. 1Ba and b). Subsequent application of 1 µM nifedipine did not affect the late inward current component, indicating that Na^+ was the predominant ion carrying the DHP-sensitive sustained inward current. At voltages positive to −20 mV the outward current component was partially reduced by nifedipine (average current density of the DHP-sensitive outward current, 0.34 ± 0.08 pA/pF at + 20 mV; n = 4, two independent experiments: N = 2), suggesting that Cs^+ was carrying the DHP-sensitive current component.

We next evaluated the kinetics of inactivation of the sustained inward current in mouse SAN cells in further detail (Fig. 1C and D). In the experiment shown in Fig. 1C, the inactivation time course was determined by measuring the fractional change of the sustained current elicited by a depolarizing step to −50 mV from a holding potential of −80 mV in 0.1 mM $[Ca^{2+}]_o$, immediately (0.05 s) before (I_{ref}) and after (I_{test}) conditioning pulses to 0 mV of variable duration (0.5–4.5 s). Nifedipine was then applied to acquire the background current (*red trace*) at −50 mV, which was used to evaluate the net amplitude of the DHP-sensitive inward current. In Fig. 1C the ratio of I_{test}/I_{ref} is plotted as a function of the conditioning pulse duration, indicating that while I_{st} displayed

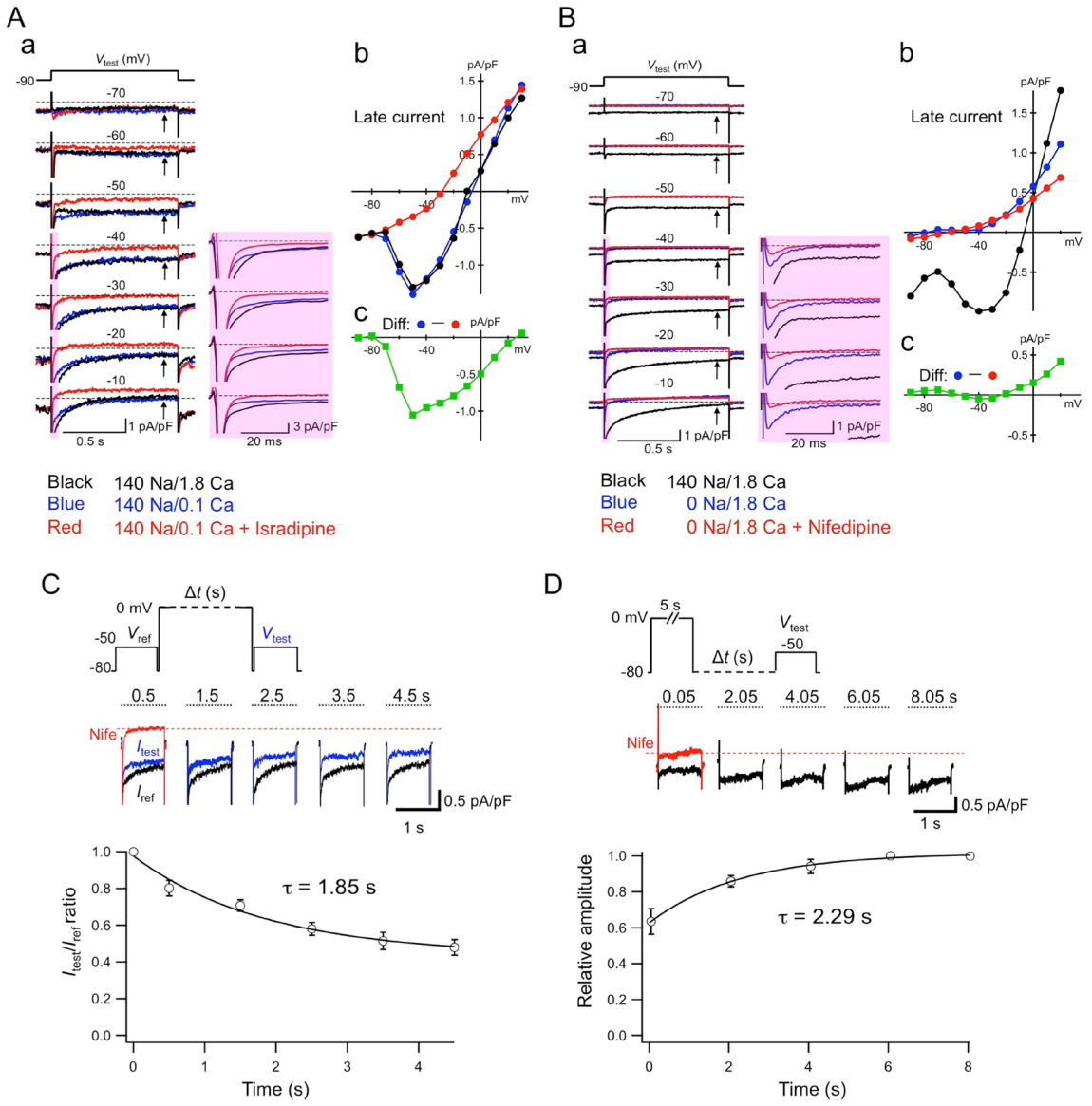

Figure 1. Presence of I_{st} in mouse SAN cells. (**A**) (a) Superimposed whole-cell membrane currents recorded from the same cell in 1.8 mM $[Ca^{2+}]_o$ (control, *black*), in 0.1 mM $[Ca^{2+}]_o$ (*blue*) and after exposure to 1 µM isradipine (*red*). Individual SAN cells were voltage clamped at a holding potential of −90 mV and depolarized for 1 s to indicated test potentials in 10-mV increments. Peaks of transient inward currents at the beginning of test pulses are not to scale. The *inset* shows close-up views of the initial part (*red shaded area*) of current traces. (**b**) Corresponding isochronal *I–V* relationships of the late current measured at time points marked with arrows in a. (c) *I–V* relationship of the isradipine-sensitive current obtained by subtraction of the current recorded after application of isradipine from that recorded in 0.1 mM $[Ca^{2+}]_o$. (**B**) (a) Superimposed whole-cell membrane currents recorded in the same cell in 1.8 mM $[Ca^{2+}]_o$ (control, *black*), in NMDG-substituted, Na^+-free solution (*blue*) and after exposure to 1 µM nifedipine (*red*) using the same pulse protocol as in (**A**). The *inset* shows close-up views of the initial part (*red shaded area*) of current traces. (b) Corresponding *I–V* relationships of the late currents from the recording depicted in a. (c) *I–V* relationship of the nifedipine-sensitive current obtained by subtraction of currents after application of nifedipine from recordings in the NMDG-substituted, Na^+-free solution. (**C**) Time dependency of the sustained inward current inactivation measured using a protocol (*upper panel*) consisting of a reference test pulse (V_{ref}), a conditioning prepulse of various durations, and a subsequent test pulse (V_{test}). Sample traces of I_{ref} (*black*) and I_{test} (*blue*) recorded in response to V_{ref} and V_{test}, respectively, in 0.1 mM $[Ca^{2+}]_o$ were superimposed. The *red* trace (Nife) was recorded in the presence of 1 µM nifedipine and indicates the background level at −50 mV (*red dash line*). The dotted line (*black*) indicates the zero-current level. The *bottom panel* shows a plot of the average ratio of I_{test}/I_{ref} as a function of the conditioning pulse duration. The continuous line represents a single exponential fit. (**D**) Time dependency of the recovery from inactivation of the sustained inward current measured using a double-pulse protocol (*upper panel*) with varying recovery intervals (0.05–8.05 s) at −80 mV between a 5-s conditioning prepulse to 0 mV and a test pulse (V_{test}) to −50 mV. Current amplitudes are normalized to the largest current obtained with a recovery interval of 8.05 s. Sample traces and panels are labelled as in (**C**).

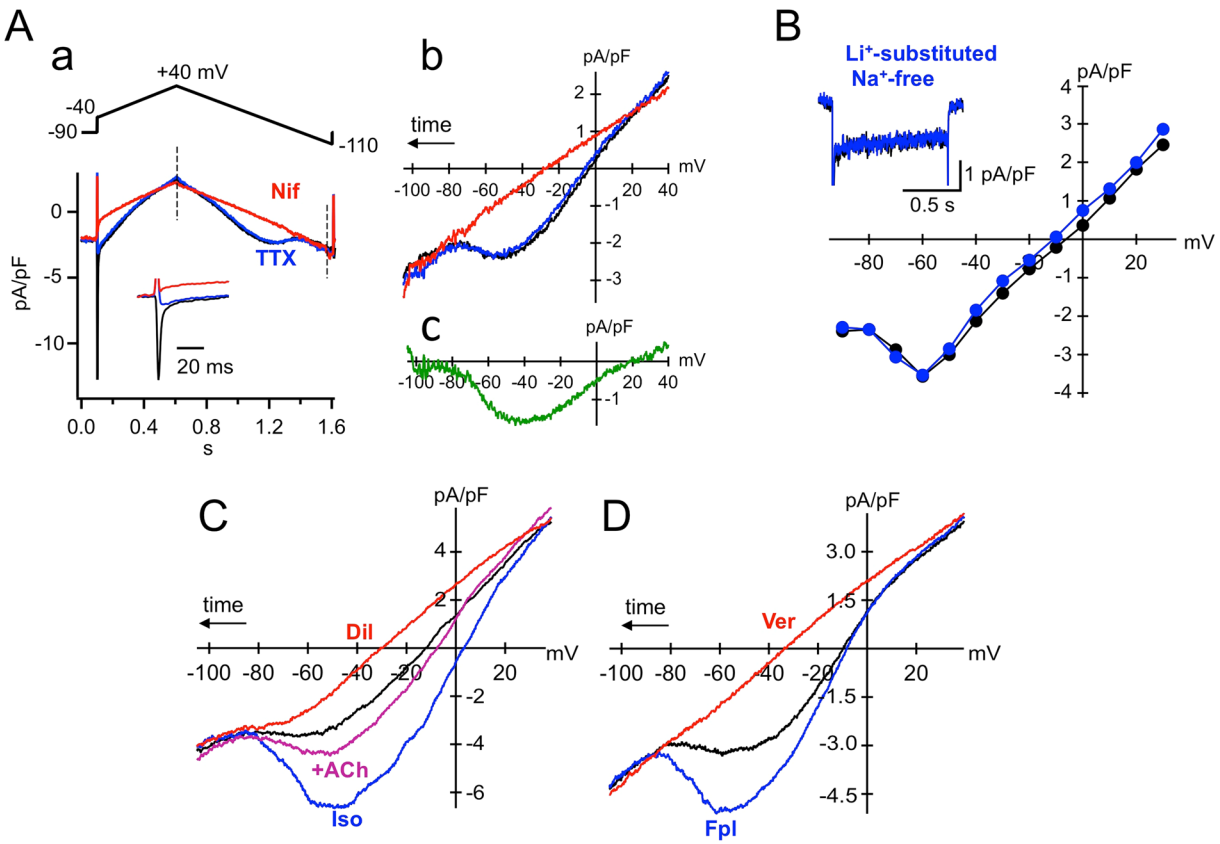

Figure 2. Pharmacological properties of I_{st} in mouse SAN cells. (**A**) Effects of TTX on I_{st}. (a) Voltage ramp pulse protocol and original current traces recorded from the same cell in 0.1 mM $[Ca^{2+}]_o$ (control, *black*), during exposure to 10 µM TTX (*blue*) and after subsequent addition of 1 µM nifedipine (*red*). The inset shows expanded traces at the beginning of the voltage-command pulse. (b) Corresponding *I–V* relationship obtained from current recordings during the descending ramp from + 40 to −110 mV in a. (c) *I–V* relationship of I_{st} isolated by subtracting current recordings before and after application of nifedipine in the presence of TTX. (**B**) Effects of Na^+ replacement with Li^+ on I_{st}. The *I–V* relationships were constructed on current recordings before (*black*) and after (*blue*) total replacement of Na^+ with Li^+ in the 0.1 mM $[Ca^{2+}]_o$ solution. Currents were elicited by 1-s depolarizing pulses (10 mV increment) to various test potentials from a holding potential of −90 mV. The inset shows original current traces at −50 mV. (**C**) Effects of autonomic agonists on I_{st}. The *I–V* relationships were obtained from current recordings in the same cell during the descending limb of a voltage ramp (similar to (**A**)) in the control 0.1 mM $[Ca^{2+}]_o$ solution (*black*), during exposure to 100 nM Iso (*blue*) and Iso plus 1 µM ACh (*purple*), and after addition of 1 µM diltiazem (Dil, *red*). (**D**) Effects of a non-DHP $I_{Ca,L}$ agonist on I_{st}. Superimposed *I–V* relationships were obtained during the descending limb of a voltage ramp (similar to (**A**)) in the control 0.1 mM $[Ca^{2+}]_o$ solution (*black*), during exposure to 1 µM FPL-64176 (Fpl, *blue*) and after subsequent addition of 1 µM verapamil (Ver, *red*).

slow inactivation ($\tau = 1.94 \pm 0.57$s, n = 3, N = 1), a considerable current fraction remained available even after a 4.5-s conditioning pulse (0.48 ± 0.04, n = 3, N = 1). In addition, recovery from inactivation was assessed by applying a 5-s conditioning prepulse followed by test pulses to −50 mV after varying intervals of recovery (0.05–8.05 s) at −80 mV (Fig. 1D). Recovery of the sustained current proceeded exponentially with a time constant of 2.66 ± 0.63s (n = 3, N = 1).

These properties (low voltage for activation, DHP sensitivity, Na^+ permeability and slow inactivation), clearly identified the sustained inward current in our mouse SAN cell preparations as I_{st}[5,15–18,26]. We only failed to record the sustained current in five of 24 experiments (~20%), which is likely to indicate inhomogeneous expression of I_{st} in SAN cells[16]. Four of five I_{st}-deficient cells were nearly indistinguishable from clear striated atrial-like myocytes.

I_{Na} and I_{NCX} do not contribute to I_{st} in mouse SAN. To assess whether voltage-gated Na^+ currents could interfere with I_{st} recordings in mouse SAN cells, we investigated the effect of the I_{Na} blocker TTX on the membrane current (Fig. 2A). Since I_{st} exhibited little inactivation during the 1-s square pulse, the *I–V* relationship was measured using a slow (150 mV/s) voltage-ramp protocol in 0.1 mM $[Ca^{2+}]_o$. Under these conditions, the contributions of $I_{Ca,L}$ and $I_{Ca,T}$ to the total membrane current were minimized[5,15,18]. Figure 2Aa shows a superimposition of the original current traces in response to the voltage ramp in the control (*black trace*), during 10 µM TTX application (*blue trace*) and after nifedipine application (*red trace*). Figure 2Ab displays the corresponding

Drugs	Concentration [μM]	I_{st}	$I_{Ca,L}$	References
Dihydropyridines				
Nicardpine	0.25–0.5	block	block	Guo *et al.*[5]
Nifedipine	0.03–1.0	block	block	this study
Isradipine	1.0	block	block	this study
Bay-K8644 (agonist)	1.0	increase	increase	Guo *et al.*[15]
Benzothiazepines				
Diltiazem	1.0	block	block	this study
Phenylalkylamines				
D600	0.1	block	block	Guo *et al.*[5]
Verapamil	1.0	block	block	this study
FPL-64176 (agonist)	1.0	increase	increase	this study
Tetrodotoxin	10–30	no effect	no effect	Guo *et al.*[5]; this study
Isoprenaline	~0.1	increase	increase	Toyoda *et al.*[18]; this study

Table 1. Pharmacological similarities between I_{st} and $I_{Ca,L}$.

I–V relationships obtained from the descending limb of the voltage ramp. As evidenced in the current recordings and in the corresponding *I–V* curve, bath application of TTX readily inhibited the transient inward I_{Na} at the beginning of the pulse (see *expanded traces in the inset*), but did not affect the subsequent current. Application of nifedipine (1 μM) then revealed that the TTX-insensitive and DHP-sensitive current component could be attributed to I_{st} (Fig. 2Ac). It should be noted that partial inhibition of the late inward current by TTX was observed in six of 23 cells (26%) (average current density of TTX-sensitive current, 0.82 ± 0.17 pA/pF at −50 mV; n = 6, N = 4), suggesting that some mouse SAN cells also express a TTX-sensitive persistent Na^+ current[27].

The involvement of I_{NCX} was also investigated (Fig. 2B). I_{st} was hardly affected by total replacement of external Na^+ with an equimolar concentration of Li^+ to abolish I_{NCX}. This result is consistent with the previously characterized selectivity of I_{st} to monovalent cations[26]. In conclusion, I_{NCX} did not contaminate our recordings of I_{st}.

Sensitivity of I_{st} to $I_{Ca,L}$ modulators in mouse SAN cells. We then characterized the pharmacological properties of I_{st} by testing its sensitivity to various $I_{Ca,L}$ modulators in the presence of 0.1 mM $[Ca^{2+}]_o$ solution. In the experiment shown in Fig. 2C, 0.1 μM isoprenaline (Iso) strongly increased I_{st} (116.1 ± 16.8%, n = 8, N = 2, p = 0.0003). This stimulatory effect was almost reversed by addition of 1 μM acetylcholine (ACh) in the presence of Iso (84.3 ± 2.7%, n = 4, N = 2, p = 0.0029). Finally, the non-DHP $I_{Ca,L}$ blocker diltiazem (1 μM) completely abolished I_{st}. By contrast, the $I_{Ca,L}$ agonist FPL-64176 (1 μM) potentiated the amplitude of I_{st} nearly twofold, whereas application of 1 μM verapamil totally abolished I_{st} (Fig. 2D). Our observations, in addition to the findings of previous studies[5,15,18], indicate that the pharmacological properties of I_{st} are undistinguishable from those of $I_{Ca,L}$ (Table 1).

I_{st} is absent in $Ca_V1.3^{-/-}$ SAN cells. The undistinguishable pharmacological properties of I_{st} and $I_{Ca,L}$ (Table 1) provided a strong rationale for testing the hypothesis that these currents share common molecular determinants. It is now generally accepted that $I_{Ca,L}$ in SAN cells is composed of two separate current components mediated by distinct pore-forming alpha subunits, $Ca_V1.2$ and $Ca_V1.3$[11,12]. To directly examine the possibility of a functional link between I_{st} and $Ca_V1.3$, we recorded $I_{Ca,L}$ and I_{st} in SAN cells from mice lacking $Ca_V1.3$ channels ($Ca_V1.3^{-/-}$ mice, Fig. 3). Since most SAN cells obtained from $Ca_V1.3^{-/-}$ mice were quiescent, we selected single cells for recordings based on morphological criteria rather than spontaneous activity. After the control recording in Cs^+-substituted, K^+-free Tyrode solution with 1.8 mM $[Ca^{2+}]_o$ (*black traces*), I_{st} was separated from $I_{Ca,L}$ by switching the bath solution to 0.1 mM $[Ca^{2+}]_o$ containing 10 μM TTX (*blue traces*). I_{st} was identified as a current component inhibited by subsequent application of 1 μM nifedipine (*red traces*). Consistent with previous studies, genetic ablation of $Ca_V1.3$ channels resulted in considerable reduction of $I_{Ca,L}$[12] as well as a shift in the current half-activation voltage[11,12] (Fig. 3A–C). Indeed, the peak density of $I_{Ca,L}$ was significantly reduced from −6.97 ± 0.85 pA/pF in wild-type SAN cells (n = 19, N = 6) to −4.81 ± 0.45 pA/pF in $Ca_V1.3^{-/-}$ cells (n = 18, N = 6, p = 0.0336), and was accompanied by a positive shift in the peak of the *I–V* relationship by ~20 mV (Fig. 3C). The calculated half-maximal activation voltage ($V_{0.5act}$) was shifted from −29.3 mV in wild-type cells to −12.8 mV in $Ca_V1.3^{-/-}$ SAN cells.

I_{st} was evident in wild-type SAN cells after $I_{Ca,L}$ removal by lowering $[Ca^{2+}]_o$, as manifested by the increase in the sustained inward current with depolarization between −70 and −50 mV that was finally blocked by nifedipine (Fig. 3A and B). By contrast, the late current obtained from $Ca_V1.3^{-/-}$ SAN cells changed linearly with command voltage in the 0.1 mM $[Ca^{2+}]_o$ solution with 10 μM TTX, and there remained no detectable DHP-sensitive current. As shown in Fig. 3D, the average peak density of I_{st} was −0.98 ± 0.09 pA/pF (n = 19, N = 6) in wild-type cells, while it was reduced below detectable levels in $Ca_V1.3^{-/-}$ cells (n = 18, N = 6). Thus, we concluded that I_{st} was virtually absent in SAN cells from $Ca_V1.3^{-/-}$ mice.

The above results suggested that $Ca_V1.3$ mediated two different currents in SAN cells, i.e. Ca^{2+}-conducting $I_{Ca,L}$ and Na^+-conducting I_{st}. To support this hypothesis and estimate the contribution of $Ca_V1.3$-mediated $I_{Ca,L}$ and I_{st} to the diastolic depolarization, $I_{Ca,L}$ and I_{st} were alternately recorded in the same cell under distinct external ionic conditions and activation in the diastolic depolarization range was evaluated in wild-type and $Ca_V1.3^{-/-}$ SAN

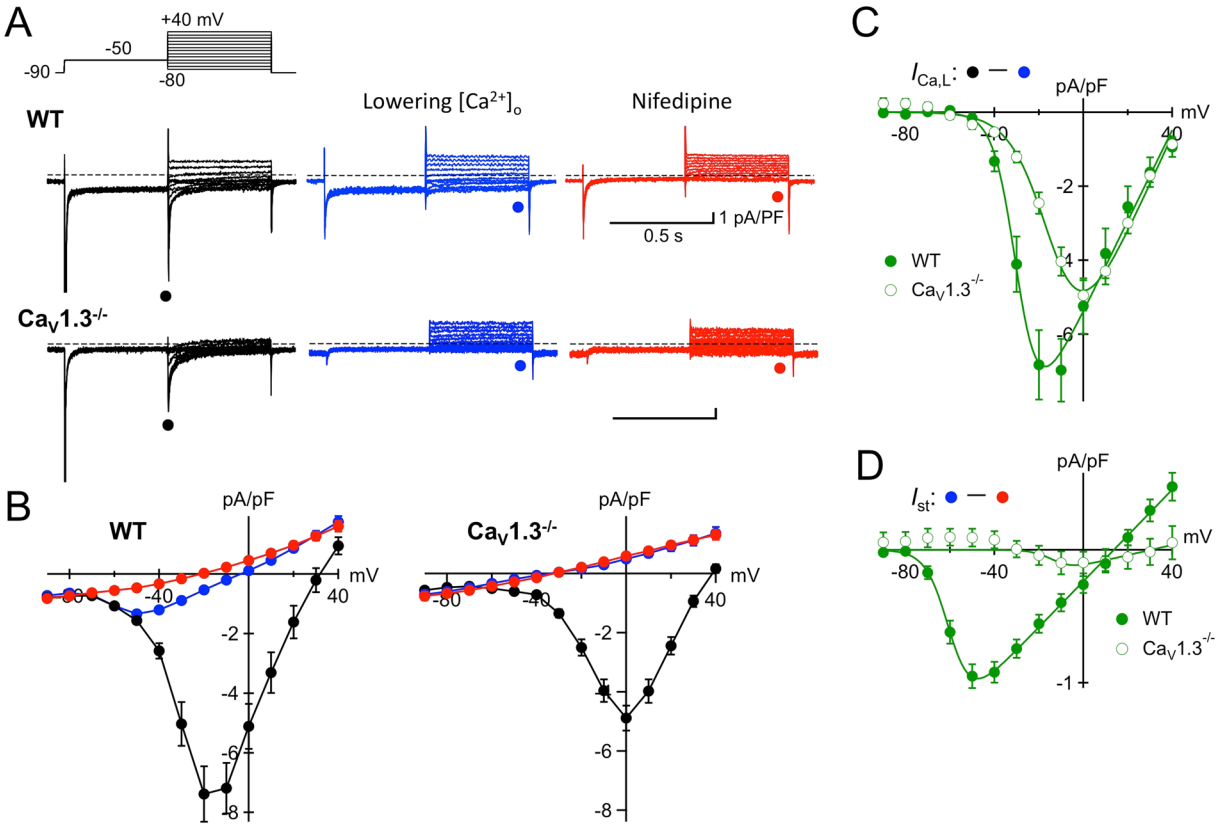

Figure 3. Absence of I_{st} in SAN cells from $Ca_V1.3^{-/-}$ mice. (**A**) Representative examples of current recordings in SAN cells obtained from wild-type (*upper panel*) and $Ca_V1.3^{-/-}$ (*lower panel*) mice. Currents were elicited by voltage steps to test potentials between −80 and + 40 mV (10 mV increments) preceded by a conditioning pulse to −50 mV from a holding potential of −90 mV in 1.8 mM $[Ca^{2+}]_o$ (control, *black*), in 0.1 mM $[Ca^{2+}]_o$ solution containing 10 µM TTX (*blue*) and after applying 1 µM nifedipine (*red*). (**B**) Average *I–V* relationships of current densities measured at the time points indicated in (**A**). Data represent the mean ± S.E.M. of wild-type (*left*, n = 19) and $Ca_V1.3^{-/-}$ (*right*, n = 18) SAN cells. (**C**), *I–V* relationships of $I_{Ca,L}$ in wild-type (*closed symbols*) and $Ca_V1.3^{-/-}$ (*open symbols*) SAN cells, obtained by subtraction of currents after lowering $[Ca^{2+}]_o$ from recordings in the control solution. (**D**) *I–V* relationships of I_{st} in wild-type (*closed symbols*) and $Ca_V1.3^{-/-}$ (*open symbols*) SAN cells, measured as the nifedipine-sensitive current in 0.1 mM $[Ca^{2+}]_o$.

cells (Fig. 4). A slow ascending ramp (−65 to −35 mV, 100 mV/s) voltage command was employed to mimic the diastolic depolarization. We first recorded $I_{Ca,L}$ using the 0 Na^+, 1.8 mM Ca^{2+} external solution (Fig. 4A). Under these recording conditions, the voltage ramp gradually activated an inward current yielding negative slope conductance in wild-type SAN cells. This current was strongly augmented by Iso and inhibited by subsequent application of nifedipine. The nifedipine-sensitive difference current showed that the net $I_{Ca,L}$ started to activate clearly within the diastolic depolarization range, as expected for the low-voltage activation of $Ca_V1.3$-mediated $I_{Ca,L}$. The average threshold for activation of $Ca_V1.3$-mediated $I_{Ca,L}$ was −51.2 ± 1.0 mV under control conditions and −59.8 ± 0.9 mV upon perfusion of Iso (n = 7, N = 3). Iso significantly augmented the amount of charge carried by $Ca_V1.3$-mediated $I_{Ca,L}$ from 0.068 ± 0.013 to 0.177 ± 0.023 pQ/pF (n = 7, N = 3, p = 0.0003). In contrast to wild-type SAN cells, significant nifedipine-sensitive $Ca_v1.3$-mediated $I_{Ca,L}$ was not recorded in $Ca_v1.3^{-/-}$ SAN cells (Fig. 4B). Similar to wild-type cells, $Ca_V1.2$-mediated $I_{Ca,L}$ could be elicited by subsequent depolarization at +10 mV. We did not find a statistically significant difference in the response of $I_{Ca,L}$ at +10 mV to Iso between wild-type (112.0 ± 8.7%, n = 7, N = 3) and $Ca_V1.3^{-/-}$ SAN cells (94.6 ± 6.1%, n = 6, N = 3, p = 0.1319). Taken together, these observations indicated that $Ca_V1.3$ channels alone fully accounted for $I_{Ca,L}$ in the pacemaker potential range.

We then switched to an external recording solution containing 140 mM Na^+, 0.1 mM Ca^{2+} and 10 µM TTX to record I_{st} in the same cells. As illustrated in Fig. 4E, slow replacement of the bathing solution enabled the monitoring of gradual changes in membrane currents. These changes included a marked inward shift in the holding current and a reduction in $I_{Ca,L}$ at +10 mV (indicated by arrows). In contrast to $I_{Ca,L}$, we observed an increase in the inward current accompanied by a negative shift in the peak potential, which indicated that increased I_{st} offsets the loss of $I_{Ca,L}$ along the voltage ramp. Similar to $I_{Ca,L}$, I_{st} was enhanced by Iso and blocked by nifedipine (Fig. 4C). I_{st} was detected in all wild-type SAN cells (0.228 ± 0.039 and 0.453 ± 0.076 pQ/pF in the absence and presence of Iso, respectively, n = 7, N = 3). However, we failed to record I_{st} in $Ca_V1.3^{-/-}$ SAN cells (0.012 ± 0.002 and 0.014 ± 0.004 pQ/pF in the absence and presence of Iso, respectively, n = 6, N = 3, Fig. 4D).

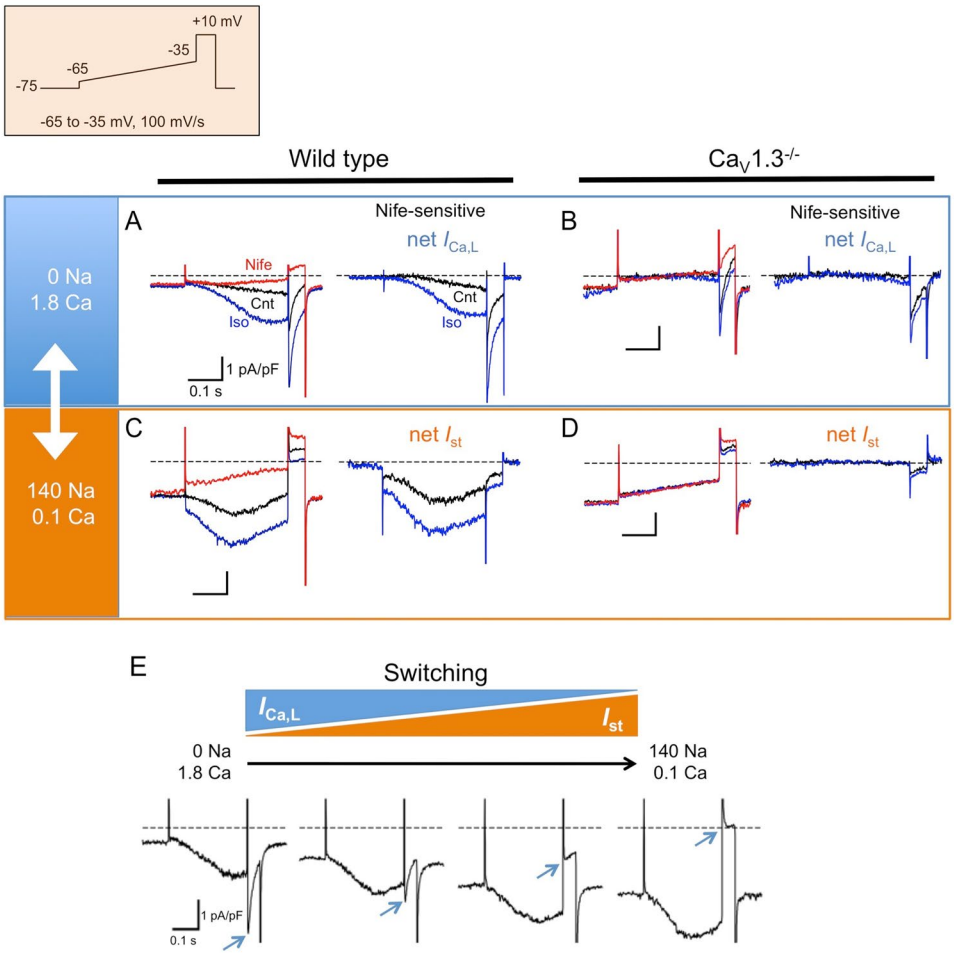

Figure 4. $Ca_V1.3$ mediates both $I_{Ca,L}$ and I_{st} in the SAN diastolic depolarization range. (**A**,**C**) Representative whole-cell membrane currents recorded from the same wild-type SAN cell using two different external solutions: TEA^+-substituted, Na^+-free external solution containing 1.8 mM Ca^{2+} (**A**) to record $I_{Ca,L}$ and 140 mM $[Na^+]_o$ solution containing 0.1 mM Ca^{2+} plus 10 μM TTX (**C**) to record I_{st}. The cell was first held at −75 mV. Then, a slow ascending ramp (100 mV/s) voltage command was used to elicit $I_{Ca,L}$ or I_{st} (*top panel*), from −65 to −35 mV, followed by depolarization to +10 mV for 50 ms. Under distinct external conditions, currents were recorded in the absence (*black trace, left panel*) and presence (*blue trace, left panel*) of 100 nM Iso, and after addition of 1 μM nifedipine (*red trace, left panel*). Nifedipine-sensitive net $I_{Ca,L}$ and I_{st} in the absence (*black trace, right panel*) and presence (*blue trace, right panel*) of Iso were obtained by digital subtraction of current traces before and after application of nifedipine (*right panel*). (**B**,**D**) Representative $I_{Ca,L}$ (**B**) and I_{st} (**D**) in $Ca_V1.3^{-/-}$ SAN cells, recorded using the same protocol as in (**A**,**C**), respectively. (**E**) Sample current recordings in a wild-type SAN cell during gradual replacement of the external solution for $I_{Ca,L}$ recording with that for I_{st} recording in the presence of Iso. Arrows indicate the peak of $I_{Ca,L}$.

We did not observe either I_{st} or $I_{Ca,L}$ in atrial-like myocytes isolated from wild-type SAN (n = 4, N = 3, data not shown). Thus, the presence of I_{st} was always coupled to the low voltage-activated $I_{Ca,L}$, which is consistent with the view that $Ca_V1.3$ mediates both $I_{Ca,L}$ and I_{st}.

$Ca_V1.2$ channels are not involved in the generation of I_{st}. The absence of I_{st} in $Ca_V1.3^{-/-}$ SAN cells does not exclude the possibility that $Ca_V1.2$ also contributes to the generation of I_{st}. To examine the involvement of $Ca_V1.2$ in I_{st}, we employed knock-in mice in which a point mutation (T1066Y) abolishes the sensitivity of $Ca_V1.2$ to DHPs without changing channel function and expression ($Ca_V1.2^{DHP-/-}$ mice, Fig. 5)[28]. In this mouse model, selective blockade of $Ca_V1.3$ by DHPs enables the functional contributions of $Ca_V1.2$ and $Ca_V1.3$ to the generation of $I_{Ca,L}$ to be distinguished. We first tested the effect of nifedipine on $I_{Ca,L}$ in SAN cells from $Ca_V1.2^{DHP-/-}$ mice (Fig. 5A). $I_{Ca,L}$ was recorded after elimination of I_{st} and I_{Na} by Na^+ removal from the external recording solution. Bath application of nifedipine (0.03–1 μM) reduced the peak amplitude of $I_{Ca,L}$ in a concentration-dependent manner to a maximum of ~64% even at a saturating concentration of DHP (1 μM). This residual DHP-resistant $I_{Ca,L}$ was completely blocked by application of verapamil (3 μM), in line with previous data showing that the T1066Y mutation preserves the high sensitivity of $Ca_V1.2$ to phenylalkylamines[29]. Peak inward current of the nifedipine-resistant component activated more slowly (Fig. 5A), as expected for $Ca_V1.2$-mediated

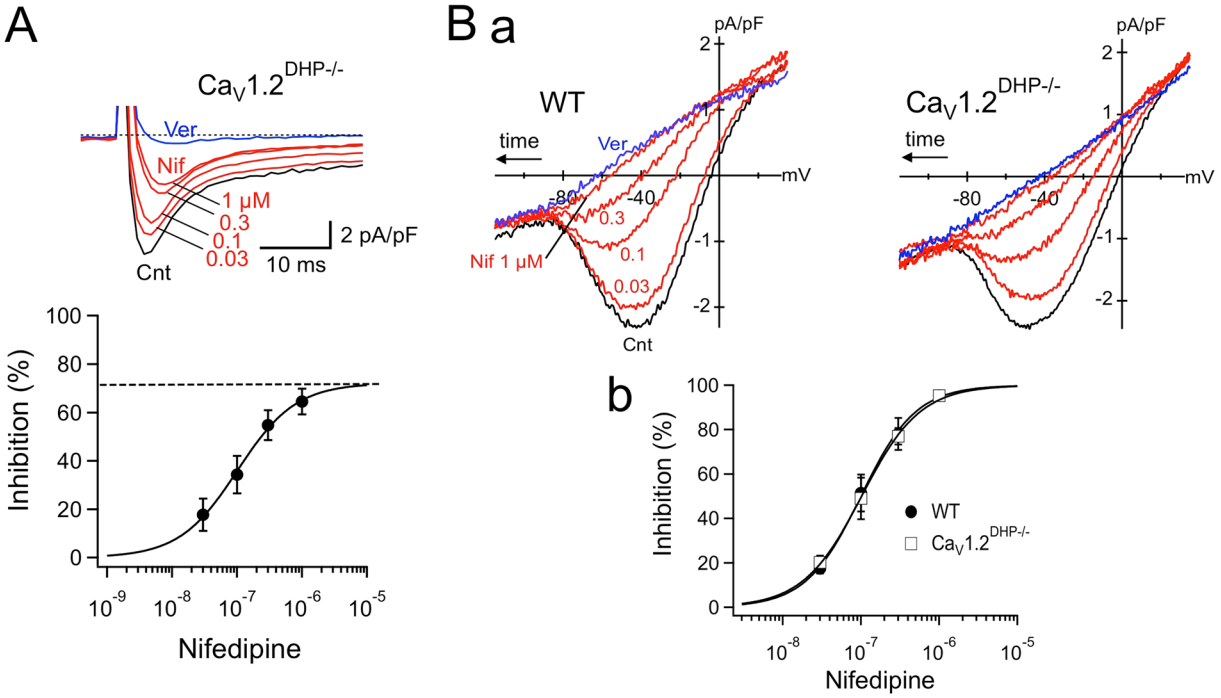

Figure 5. Sensitivity of $I_{Ca,L}$ and I_{st} to nifedipine in SAN cells from Ca$_V$1.2$^{DHP-/-}$ mice. (**A**) $I_{Ca,L}$ inhibition by nifedipine in Ca$_V$1.2$^{DHP-/-}$ SAN cells. (a) Superimposed sample traces of $I_{Ca,L}$ elicited by depolarization to −10 mV from a holding potential of −50 mV in TEA$^+$-substituted, Na$^+$-free Tyrode solution (control, *black*) and during nifedipine application at various concentrations (0.03–1 μM, *red*), and after subsequent addition of 3 μM verapamil (*blue*). (b) Concentration-dependent inhibition of $I_{Ca,L}$ by nifedipine. Inhibition is expressed as the percentage of residual $I_{Ca,L}$ inhibited by nifedipine relative to control $I_{Ca,L}$. Data are mean ± S.E.M. of four experiments. The smooth curve represents the least squares fit of data points using the Hill equation, yielding a maximal current response of 72%, IC_{50} of 101.7 nM and Hill coefficient of 0.97. (**B**) Effects of nifedipine on I_{st} in wild-type and Ca$_V$1.2$^{DHP-/-}$ SAN cells. (a) Superimposed *I–V* relationships of I_{st} obtained by voltage ramp in wild-type (*left*) and Ca$_V$1.2$^{DHP-/-}$ (*right*) SAN cells in the control 0.1 mM $[Ca^{2+}]_o$ solution (control, *black*), during exposure to various concentrations of nifedipine (0.03–1 μM, *red*), and after application of 3 μM verapamil (*blue*). (b) Concentration–response relationship of I_{st} inhibition by nifedipine in wild-type (*closed circles*) and Ca$_V$1.2$^{DHP-/-}$ (*open squares*) SAN cells. Data are mean ± S.E.M. of four independent measurements. The line represents the fit of the Hill equation.

$I_{Ca,L}$[30]. The presence of this DHP-insensitive component is consistent with our earlier finding[11,12] that $I_{Ca,L}$ in SAN cells is mediated by both Ca$_V$1.2 and Ca$_V$1.3.

We then examined whether altered sensitivity of Ca$_V$1.2 to DHP also affected the response of I_{st} to nifedipine. The concentration-dependent inhibition of I_{st} by nifedipine was investigated in SAN cells isolated from wild-type and Ca$_V$1.2$^{DHP-/-}$ mice (Fig. 5B). After suppressing $I_{Ca,L}$ by lowering $[Ca^{2+}]_o$ to 0.1 mM, I_{st} was elicited by the voltage ramp in the presence of nifedipine at various concentrations (0.03–1 μM). I_{st} in Ca$_V$1.2$^{DHP-/-}$ SAN cells was reduced by nifedipine to levels similar to those observed in wild-type cells. Indeed, we failed to detect a nifedipine-resistant I_{st} component at 1 μM. Fitting the concentration–response relationship to the Hill equation gave a half-maximal inhibitory concentration (IC_{50}) value of 118.5 ± 28.8 nM (n = 4, N = 4) in Ca$_V$1.2$^{DHP-/-}$ SAN cells, similar to the value of 129.1 ± 28.8 nM (n = 4, N = 4) in wild-type cells. Thus, it is unlikely that Ca$_V$1.2 confers the structural basis for I_{st} sensitivity to DHPs. Of interest, the IC_{50} for I_{st} was close to that for $I_{Ca,L}$ in Ca$_V$1.2$^{DHP-/-}$ SAN cells (104.2 ± 26.6 nM, n = 4, N = 4, Fig. 5A), suggesting that Ca$_V$1.3 is responsible for the DHP sensitivity of I_{st}.

Discussion

Here we have demonstrated, for the first time, that voltage-gated L-type Ca$_V$1.3 Ca^{2+} channels are essential for the expression of a DHP-sensitive, voltage-dependent Na^+ conductance, previously described as I_{st}. Our finding is based on the observations that (1) I_{st} is consistently identified in wild-type SAN cells but not in Ca$_V$1.3-deficient cells; (2) block of I_{st} by nifedipine was unaffected upon ablation of Ca$_V$1.2 DHP sensitivity in Ca$_V$1.2$^{DHP-/-}$ SAN cells; (3) DHP sensitivity of I_{st} overlapped that of Ca$_V$1.3-mediated $I_{Ca,L}$ in Ca$_V$1.2$^{DHP-/-}$ SAN cells; and (4) I_{st} could not be attributed to late I_{Na} or I_{NCX}. Sensitivity to Ca^{2+}-channel blockers such as DHPs, verapamil and diltiazem, as well as activators such as Bay-K8644 and FPL-64176, is based on highly specialized structural motifs conserved in Ca$_V$1 α_1-subunits of L-type Ca^{2+} channels[21,31]. Thus, our genetic and pharmacological evidence showing overlapping properties between I_{st} and Ca$_V$1.3-mediated $I_{Ca,L}$ indicates a close functional relationship between these currents in SAN cells (Table 1). The demonstration of Ca$_V$1.3 α_1-subunits as essential molecular determinants of

a voltage-dependent DHP-sensitive Na^+ conductance is a novel and unexpected finding and constitutes a fundamental step in elucidating the molecular nature of I_{st}.

Our patch-clamp recordings clearly show that under physiological conditions I_{st} is predominantly carried by Na^+ rather than Ca^{2+} ions. Indeed, while lowering external Ca^{2+} did not affect I_{st}, removal of extracellular Na^+ abolished the current even in the presence of a physiological concentration of Ca^{2+} (Fig. 1). L-type Ca^{2+} channels are permeable to Na^+ in the absence of extracellular divalent cations[32,33]. However, L-type Ca^{2+} channels are highly selective for Ca^{2+} over Na^+ with a permeation ratio (P_{Ca}/P_{Na}) of ~1000 under physiological conditions[32]. Therefore, Na^+ influx through L-type Ca^{2+} channels is blocked by extracellular Ca^{2+} in the submicromolar range[32,33]. It is thus unlikely that the "classical" permeation pathway of L-type Ca^{2+} channels mediates I_{st}. Indeed, currently available recombinant $Ca_V1.3$ channels with canonical channel pore sequence are Ca^{2+}-selective $I_{Ca,L}$, with poor permeability to Na^+ at least in the experimental solutions used for the I_{st} recording in the present study (Toyoda *et al.*, unpublished observation). Our results therefore suggest that $Ca_V1.3$ α_1-subunits in the SAN cell not only form $Ca_V1.3$ L-type channels but also contribute to the formation of voltage-gated Na^+ conductance through an unknown mechanism.

However, revealing the molecular mechanism allowing $Ca_V1.3$ α_1-subunits to form I_{st} is challenging. We favour the hypothesis that $Ca_V1.3$ α_1-subunits themselves form the I_{st} pore due to the observation that I_{st} and $Ca_V1.3$ possess an essentially indistinguishable pharmacological profile and Ca^{2+}-channel blockers have been shown to exert their pharmacological modulation exclusively by binding to α_1-subunits[34]. In this case the different ion selectivity of I_{st} in SAN cells would require a modification of the ion permeation pathway. Substitution of negatively charged residues forming the ion selectivity filter of voltage-gated Ca^{2+} channels by lysine can indeed induce persistent Na^+ currents similar to I_{st}[35,36], suggesting that increased Na^+ permeability *per se* could reproduce I_{st} properties. To date, analysis of $Ca_V1.3$ transcripts has not identified alternatively spliced $Ca_V1.3$ variants with a modified selectivity filter[37–39]. Since Na^+ conductance through such modified channels may be larger than for Ca^{2+} [36,40], I_{st} transcripts may be present at low levels. This would make their detection particularly difficult in tissues with low cell numbers such as the SAN. On the other hand, the possibility that I_{st} could be generated by alternative splicing of Ca^{2+} channels is also suggested by a recent report that T-type (Ca_V3) Ca^{2+} channels of the snail heart have high permeability to Na^+ due to unique splicing in the outer pore region[41]. Although this possibility cannot be excluded for mammalian SAN, splicing of T-type α_1-subunits appears an unlikely explanation for I_{st} because of the L-type channel-specific pharmacology. Another possible explanation for Na^+ selectivity of $Ca_V1.3$ α_1-subunits could be structural modifications of the ion conducting pathway through RNA editing, which so far has only been detected in the brain and in the cytoplasmic C-terminal tail of the channel[39,42].

Alternatively, a cationic channel functionally coupled to $Ca_V1.3$ activity could mediate I_{st}. In mouse SAN cells $Ca_V1.3$ is co-localized with sarcoplasmic reticulum ryanodine receptors (RyRs) and controls diastolic RyR-dependent Ca^{2+} release[25,43]. RyR-dependent Ca^{2+} release could then activate an inward Na^+ current. However, the possibility that I_{st} is mediated by Ca^{2+}-dependent opening of a cationic channel appears unlikely, because I_{st} density did not decrease upon lowering extracellular Ca^{2+} (Fig. 1), as one would expect for Ca^{2+}-dependent opening of a Na^+-selective channel associated with $Ca_V1.3$. Finally, the possibility that I_{st} could be generated by direct opening of a Na^+ channel physically coupled to $Ca_V1.3$ channel gating is also unlikely, because I_{st} activates negative to $Ca_V1.3$-mediated $I_{Ca,L}$ (Fig. 1).

$Ca_V1.3$ loss-of-function in mice or humans results in SAN dysfunction, which indicates that $Ca_V1.3$ channels play a major role in pacemaker activity[11,12,44–46]. Consequently, the present findings also suggest that the loss of I_{st} could contribute to the SAN dysfunction induced by $Ca_V1.3$ gene inactivation. In addition, our results indicate that the heart rate reducing effect of Ca^{2+} channel antagonists can be explained by drug binding to $Ca_V1.3$ channels and reduction of $Ca_V1.3$-mediated $I_{Ca,L}$ and I_{st}. Consistent with previous observations[11,12], our recordings in $Ca_V1.3^{-/-}$ SAN cells show that $Ca_V1.3$ underlies a low-threshold $I_{Ca,L}$ activated at voltages spanning the diastolic depolarization range. I_{st} differs from $Ca_V1.3$-mediated $I_{Ca,L}$ in the charge carrier and shows a more negative voltage for half-activation. I_{st} and $Ca_V1.3$-mediated $I_{Ca,L}$ could thus differentially contribute to the generation of the diastolic depolarization. For example, I_{st} could generate a persistent Na^+ influx in the diastolic depolarization, while $Ca_V1.3$-mediated $I_{Ca,L}$ could generate inward Ca^{2+} current[12] and control RyR-dependent Ca^{2+} release[43]. Notably, both I_{st} and $Ca_V1.3$-mediated $I_{Ca,L}$ are strongly potentiated by β-adrenergic activation, which suggests a dual role of $Ca_V1.3$ in the sympathetic control of heart rate via $I_{Ca,L}$ and I_{st}.

In conclusion, we provide novel evidence supporting the involvement of $Ca_V1.3$ in the generation of I_{st} in SAN cells. Our work provides valuable new insights into the molecular basis of I_{st} as well as the diverse functional significance of $Ca_V1.3$ in cardiac pacemaker activity.

Methods

Ethics. The investigation conforms to the Guide for the Care and Use of Laboratory Animals (8th edition, 2011), published by the US National Institutes of Health and European directives (2010/63/EU). The experimental protocol was approved by the Institutional Animal Care and Use Committee of Shiga University of Medical Science (Nos 2009-5-11, 2012-1-10 and 2014-12-3), the University of Montpellier and the University of Innsbruck.

$Ca_V1.3^{-/-}$ and $Ca_V1.2^{DHP-/-}$ mice. $Ca_V1.3^{-/-}$ and $Ca_V1.2^{DHP-/-}$ mice were obtained by crossing mice from the original mutant colonies[28,44] with mice with a C57B6/J genetic background from Charles River in the animal facility, free of specific pathogenic organisms, of the Réseau d'Animalèrie de Montpellier (RAM) at the Institut de Génetique Humaine (Montpellier, France). We next backcrossed the offspring for 10 generations with C57B6/J mice before starting the study. Animals were given *ad libitum* access to food and drinking water and were maintained in a 12-h light–dark cycle (light, 8:30 a.m. to 8:30 p.m.). Only homozygous $Ca_V1.3^{-/-}$ and $Ca_V1.2^{DHP-/-}$ mice were used for the experiments.

SAN cell preparations. Isolation of single SAN cells from mouse hearts was performed according to the methods of Mangoni and Nargeot[47]. Wild-type (N = 18), $Ca_V1.3^{-/-}$ (N = 10) and $Ca_V1.2^{DHP-/-}$ (N = 5) mice were anaesthetized with ketamine (100 mg/kg) combined with xylazine (10 mg/kg), and anticoagulated with heparin (250 units/mouse). Beating hearts were quickly removed and the SAN region was excised and cut into small strips in warm (35 °C) Tyrode solution containing (in mM): 140.0 NaCl, 5.4 KCl, 1.8 $CaCl_2$, 1.0 $MgCl_2$, 5.0 HEPES-NaOH and 5.5 D-glucose (adjusted to pH 7.4 with NaOH). The SAN tissue strips were then transferred to a low-Ca^{2+}, low-Mg^{2+} solution containing (in mM): 140.0 NaCl, 5.4 KCl, 0.5 $MgCl_2$, 0.2 $CaCl_2$, 1.2 KH_2PO_4, 50.0 taurine, 5.5 D-glucose and 5.0 HEPES-NaOH with 1.0 mg/ml bovine serum albumin (BSA) (adjusted to pH 6.9 with NaOH), and then subjected to digestion by adding Liberase TH (0.1 mg/ml, Roche Diagnostics GmBH) and elastase (1.9 U/ml, Worthington Biochem. Co.) at 35 °C for a variable time of 9–14 min. Tissue strips were then transferred and washed in a Kraft-Bruhe (KB) solution containing (in mM): 70.0 L-glutamic acid, 20.0 KCl, 80.0 KOH, 10.0 (±) D-β-OH-butyric acid, 10.0 KH_2PO_4, 10.0 taurine and 10.0 HEPES-KOH, with 1 mg/ml BSA (pH adjusted to 7.4 with KOH). SAN cells were manually dissociated by agitation using a flame-forged Pasteur pipette in KB solution at 35 °C for ~5 min. Cellular automaticity was recovered by readapting the cells to physiological extracellular Na^+ and Ca^{2+} concentrations by adding aliquots of solutions containing (in mM): 10.0 NaCl, 1.8 $CaCl_2$ and, subsequently, normal Tyrode solution containing 1 mg/ml BSA. The final storage solution contained (in mM): 100.0 NaCl, 35.0 KCl, 1.3 $CaCl_2$, 0.7 $MgCl_2$, 14.0 L-glutamic acid, 2.0 (±) D-β-OH-butyric acid, 2.0 KH_2PO_4 and 2.0 taurine, with 1.0 mg/ml BSA (pH 7.4). Cells were harvested in custom-made recording Plexiglass chambers with glass bottoms for proper cell attachment and rinsed with normal Tyrode solution warmed to 36 °C just before patch-clamp recording.

Whole-cell patch-clamp technique and data analysis. Isolated SAN cells were voltage-clamped using the whole-cell configuration of the patch-clamp technique with an EPC-8 patch-clamp amplifier equipped with an LIH-1600 AD/DA interface (HEKA) controlled by PatchMaster software or an Axon MultiClamp 700 A amplifier equipped with Digidata 1332 A interface-controlled PClamp software. Patch electrodes had a resistance of 2.5–4.0 MΩ when filled with the Cs^+-rich intracellular solution containing (in mM): 125 CsOH, 20 tetraethylammonium chloride (TEA-Cl), 1.2 $CaCl_2$, 5 Mg-ATP, 0.1 Li_2-GTP, 5.0 EGTA and 10.0 HEPES (pH adjusted to 7.2 with aspartate). The concentration of free Ca^{2+} in the pipette solutions was calculated to be approximately 4.8×10^{-8} M (pCa = 7.3). The Cs^+-substituted, K^+-free external Tyrode solution contained (in mM): 140.0 NaCl, 5.4 CsCl, 1.8 $CaCl_2$, 0.5 $MgCl_2$, 0.33 NaH_2PO_4, 5.5 glucose and 5.0 HEPES (pH adjusted to 7.4 with NaOH). The concentration of $CaCl_2$ in the external solution was reduced from 1.8 to 0.1 mM to separate I_{st} from $I_{Ca,L}$. In some experiments, NaCl was totally substituted with NMDG-Cl, TEA-Cl or LiCl. All experiments were performed at 34–36 °C.

Chemicals. Isradipine, nifedipine, verapamil, diltiazem, FPL-64176, Iso and ACh were purchased from Sigma-Aldrich. Drugs were prepared as 10 mM stock solutions in DMSO and then diluted in the external solution. TTX (Wako Chemical Co.) was dissolved in distilled water at a concentration of 10 mM and then diluted to the final concentration of 10 μM in the experimental solution.

Statistical analysis. The results are expressed as mean ± S.E.M. Statistical comparison among the different groups was performed by one-way ANOVA followed by Tukey's post-hoc HSD test. Statistical comparison between two groups was evaluated using Student's t-test. N indicates the number of hearts and n indicates the number of cells used in experiments. A p value < 0.05 was considered statistically significant.

Data availability. The datasets generated and/or analysed during the current study are available from the corresponding author upon request.

References

1. Mangoni, M. E. & Nargeot, J. Genesis and regulation of the heart automaticity. *Physiol Rev* **88**, 919–982, doi:10.1152/physrev.00018.2007 (2008).
2. DiFrancesco, D., Ferroni, A., Mazzanti, M. & Tromba, C. Properties of the hyperpolarizing-activated current (i_f) in cells isolated from the rabbit sino-atrial node. *J Physiol* **377**, 61–88 (1986).
3. Hagiwara, N., Irisawa, H. & Kameyama, M. Contribution of two types of calcium currents to the pacemaker potentials of rabbit sino-atrial node cells. *J Physiol* **395**, 233–253 (1988).
4. Verheijck, E. E., van Ginneken, A. C., Wilders, R. & Bouman, L. N. Contribution of L-type Ca^{2+} current to electrical activity in sinoatrial nodal myocytes of rabbits. *Am J Physiol* **276**, H1064–1077 (1999).
5. Guo, J., Ono, K. & Noma, A. A sustained inward current activated at the diastolic potential range in rabbit sino-atrial node cells. *J Physiol* **483**, 1–13 (1995).
6. Lakatta, E. G., Maltsev, V. A. & Vinogradova, T. M. A coupled SYSTEM of intracellular Ca^{2+} clocks and surface membrane voltage clocks controls the timekeeping mechanism of the heart's pacemaker. *Circ Res* **106**, 659–673, doi:10.1161/CIRCRESAHA.109.206078 (2010).
7. Ludwig, A. *et al.* Absence epilepsy and sinus dysrhythmia in mice lacking the pacemaker channel HCN2. *EMBO J* **22**, 216–224, doi:10.1093/emboj/cdg032 (2003).
8. Mesirca, P. *et al.* Cardiac arrhythmia induced by genetic silencing of 'funny' (*f*) channels is rescued by *GIRK4* inactivation. *Nat Commun* **5**, 4664, doi:10.1038/ncomms5664 (2014).
9. Herrmann, S., Stieber, J., Stockl, G., Hofmann, F. & Ludwig, A. HCN4 provides a 'depolarization reserve' and is not required for heart rate acceleration in mice. *EMBO J* **26**, 4423–4432, doi:10.1038/sj.emboj.7601868 (2007).
10. Baruscotti, M. *et al.* Deep bradycardia and heart block caused by inducible cardiac-specific knockout of the pacemaker channel gene. *Hcn4. Proc Natl Acad Sci USA* **108**, 1705–1710, doi:10.1073/pnas.1010122108 (2011).
11. Zhang, Z. *et al.* Functional roles of $Ca_v1.3$ (α_{1D}) calcium channel in sinoatrial nodes: insight gained using gene-targeted null mutant mice. *Circ Res* **90**, 981–987 (2002).
12. Mangoni, M. E. *et al.* Functional role of L-type $Ca_v1.3$ Ca^{2+} channels in cardiac pacemaker activity. *Proc Natl Acad Sci USA* **100**, 5543–5548, doi:10.1073/pnas.0935295100 (2003).

13. Mangoni, M. E. *et al*. Bradycardia and slowing of the atrioventricular conduction in mice lacking $Ca_V3.1/\alpha_{1G}$ T-type calcium channels. *Circ Res* **98**, 1422–1430, doi:10.1161/01.RES.0000225862.14314.49 (2006).
14. Gao, Z. *et al*. Genetic inhibition of Na^+-Ca^{2+} exchanger current disables fight or flight sinoatrial node activity without affecting resting heart rate. *Circ Res* **112**, 309–317, doi:10.1161/CIRCRESAHA.111.300193 (2013).
15. Guo, J., Mitsuiye, T. & Noma, A. The sustained inward current in sino-atrial node cells of guinea-pig heart. *Pflugers Arch* **433**, 390–396 (1997).
16. Shinagawa, Y., Satoh, H. & Noma, A. The sustained inward current and inward rectifier K^+ current in pacemaker cells dissociated from rat sinoatrial node. *J Physiol* **523**, 593–605 (2000).
17. Cho, H. S., Takano, M. & Noma, A. The electrophysiological properties of spontaneously beating pacemaker cells isolated from mouse sinoatrial node. *J Physiol* **550**, 169–180, doi:10.1113/jphysiol.2003.040501 (2003).
18. Toyoda, F., Ding, W. G. & Matsuura, H. Responses of the sustained inward current to autonomic agonists in guinea-pig sino-atrial node pacemaker cells. *Br J Pharmacol* **144**, 660–668, doi:10.1038/sj.bjp.0706101 (2005).
19. Mitsuiye, T., Shinagawa, Y. & Noma, A. Sustained inward current during pacemaker depolarization in mammalian sinoatrial node cells. *Circ Res* **87**, 88–91 (2000).
20. Catterall, W. A. & Swanson, T. M. Structural basis for pharmacology of voltage-gated sodium and calcium channels. *Mol Pharmacol* **88**, 141–150, doi:10.1124/mol.114.097659 (2015).
21. Striessnig, J. *et al*. Structural basis of drug binding to L Ca^{2+} channels. *Trends Pharmacol Sci* **19**, 108–115 (1998).
22. Catterall, W. A. Voltage-gated calcium channels. *Cold Spring Harb Perspect Biol* **3**, a003947, doi:10.1101/cshperspect.a003947 (2011).
23. Takimoto, K., Li, D., Nerbonne, J. M. & Levitan, E. S. Distribution, splicing and glucocorticoid-induced expression of cardiac α_{1C} and α_{1D} voltage-gated Ca^{2+} channel mRNAs. *J Mol Cell Cardiol* **29**, 3035–3042, doi:10.1006/jmcc.1997.0532 (1997).
24. Qu, Y., Baroudi, G., Yue, Y., El-Sherif, N. & Boutjdir, M. Localization and modulation of α_{1D} (Cav1.3) L-type Ca channel by protein kinase A. *Am J Physiol Heart Circ Physiol* **288**, H2123–2130, doi:10.1152/ajpheart.01023.2004 (2005).
25. Christel, C. J. *et al*. Distinct localization and modulation of $Ca_v1.2$ and $Ca_v1.3$ L-type Ca^{2+} channels in mouse sinoatrial node. *J Physiol* **590**, 6327–6342, doi:10.1113/jphysiol.2012.239954 (2012).
26. Guo, J., Ono, K. & Noma, A. Monovalent cation conductance of the sustained inward current in rabbit sinoatrial node cells. *Pflugers Arch* **433**, 209–211 (1996).
27. Sakmann, B. F., Spindler, A. J., Bryant, S. M., Linz, K. W. & Noble, D. Distribution of a persistent sodium current across the ventricular wall in guinea pigs. *Circ Res* **87**, 910–914 (2000).
28. Sinnegger-Brauns, M. J. *et al*. Isoform-specific regulation of mood behavior and pancreatic beta cell and cardiovascular function by L-type Ca^{2+} channels. *J Clin Invest* **113**, 1430–1439, doi:10.1172/JCI20208 (2004).
29. Huber, I. G. *et al*. Opposite effects of a single IIIS5 mutation on phenylalkylamine and dihydropyridine interaction with L-type Ca^{2+} channels. *J Biol Chem* **279**, 55211–55217, doi:10.1074/jbc.M409008200 (2004).
30. Koschak, A. *et al*. α_{1D} ($Ca_v1.3$) subunits can form l-type Ca^{2+} channels activating at negative voltages. *J Biol Chem* **276**, 22100–22106, doi:10.1074/jbc.M101469200 (2001).
31. Catterall, W. A. & Striessnig, J. Receptor sites for Ca^{2+} channel antagonists. *Trends Pharmacol Sci* **13**, 256–262 (1992).
32. Hess, P., Lansman, J. B. & Tsien, R. W. Calcium channel selectivity for divalent and monovalent cations. Voltage and concentration dependence of single channel current in ventricular heart cells. *J Gen Physiol* **88**, 293–319 (1986).
33. Matsuda, H. Sodium conductance in calcium channels of guinea-pig ventricular cells induced by removal of external calcium ions. *Pflugers Arch* **407**, 465–475 (1986).
34. Tang, L. *et al*. Structural basis for inhibition of a voltage-gated Ca^{2+} channel by Ca^{2+} antagonist drugs. *Nature* **537**, 117–121, doi:10.1038/nature19102 (2016).
35. Mikala, G., Bahinski, A., Yatani, A., Tang, S. & Schwartz, A. Differential contribution by conserved glutamate residues to an ion-selectivity site in the L-type Ca^{2+} channel pore. *FEBS Lett* **335**, 265–269 (1993).
36. Tang, S. *et al*. Molecular localization of ion selectivity sites within the pore of a human L-type cardiac calcium channel. *J Biol Chem* **268**, 13026–13029 (1993).
37. Huang, H., Yu, D. & Soong, T. W. C-terminal alternative splicing of $Ca_V1.3$ channels distinctively modulates their dihydropyridine sensitivity. *Mol Pharmacol* **84**, 643–653, doi:10.1124/mol.113.087155 (2013).
38. Safa, P., Boulter, J. & Hales, T. G. Functional properties of Cav1.3 (α_{1D}) L-type Ca^{2+} channel splice variants expressed by rat brain and neuroendocrine GH_3 cells. *J Biol Chem* **276**, 38727–38737, doi:10.1074/jbc.M103724200 (2001).
39. Huang, H. *et al*. RNA editing of the IQ domain in Cav1.3 channels modulates their Ca^{2+}-dependent inactivation. *Neuron* **73**, 304–316, doi:10.1016/j.neuron.2011.11.022 (2012).
40. Yang, J., Ellinor, P. T., Sather, W. A., Zhang, J. F. & Tsien, R. W. Molecular determinants of Ca^{2+} selectivity and ion permeation in L-type Ca^{2+} channels. *Nature* **366**, 158–161, doi:10.1038/366158a0 (1993).
41. Senatore, A., Guan, W., Boone, A. N. & Spafford, J. D. T-type channels become highly permeable to sodium ions using an alternate extracellular turret region (S5-P) outside the selectivity filter. *J Biol Chem* **289**, 11952–11969, doi:10.1074/jbc.M114.551473 (2014).
42. Danecek, P. *et al*. High levels of RNA-editing site conservation amongst 15 laboratory mouse strains. *Genome Biol* **13**, 26, doi:10.1186/gb-2012-13-4-r26 (2012).
43. Torrente, A. G. *et al*. L-type Cav1.3 channels regulate ryanodine receptor-dependent Ca^{2+} release during sino-atrial node pacemaker activity. *Cardiovasc Res* **109**, 451–461, doi:10.1093/cvr/cvw006 (2016).
44. Platzer, J. *et al*. Congenital deafness and sinoatrial node dysfunction in mice lacking class D L-type Ca^{2+} channels. *Cell* **102**, 89–97 (2000).
45. Baig, S. M. *et al*. Loss of $Ca_V1.3$ (*CACNA1D*) function in a human channelopathy with bradycardia and congenital deafness. *Nat Neurosci* **14**, 77–84, doi:10.1038/nn.2694 (2011).
46. Qu, Y., Baroudi, G., Yue, Y. & Boutjdir, M. Novel molecular mechanism involving α_{1D} (Cav1.3) L-type calcium channel in autoimmune-associated sinus bradycardia. *Circulation* **111**, 3034–3041, doi:10.1161/CIRCULATIONAHA.104.517326 (2005).
47. Mangoni, M. E. & Nargeot, J. Properties of the hyperpolarization-activated current (I_f) in isolated mouse sino-atrial cells. *Cardiovasc Res* **52**, 51–64 (2001).

Acknowledgements

The project was supported by the Grant-in-Aid for Scientific Research (C) 23590258, 26460295 and 17K08537 from the Japan Society for the Promotion of Science (to F.T.), the Agence Nationale pour la Recherche grants ANR-2010-BLAN-1128-01 and ANR-13-BSV1-023 (to M.E.M.) and the Austrian Science Fund (FWF, P27809). The IGF group is a member of the Laboratory of Excellence "Ion Channel Science and Therapeutics" (ICST) supported by a grant from ANR (ANR-11-LABX-0015). The authors are indebted to Isabelle Bidaud and to the staff of the RAM animal facility of Montpellier for technical assistance and management of the mouse lines.

Author Contributions

The experiments presented in this study were performed at the Shiga University of Medical Science and the Institut de Génomique Fonctionnelle, CNRS, UMR-5203, Inserm U 1191 in Montpellier. Specific contributions are as follows: conception and design of experiments: F.T., M.E.M. and H.M.; collection, analysis and interpretation of data: F.T., P.M., S.D., W.-G.D., M.E.M. and H.M.; drafting the manuscript and revising it critically for important intellectual content: F.T., J.S., M.E.M. and H.M. All authors critically revised the manuscript for technical and important contents.

Additional Information

Competing Interests: The authors declare that they have no competing interests.

Publisher's note: Springer Nature remains neutral with regard to jurisdictional claims in published maps and institutional affiliations.